Adsorption 8: 279–289, 2002

Adsorption of Sulfur Dioxide from Pseudo Binary Mixtures on Hydrophobic Zeolites: Modeling of the Breakthrough Curves

MARCUS MELLO AND MLADEN EIĆ*
Department of Chemical Engineering, P.O. Box 4400, University of New Brunswick, Fredericton, NB, Canada, E3B 5A3
meic@unb.ca

Received May 11, 2001; Revised July 22, 2002; Accepted August 1, 2002

Abstract. The adsorption of SO_2 from pseudo binary mixtures with water and CO_2 on hydrophobic zeolites (MFI and MOR type) was investigated using the breakthrough curve method. The SO_2 and water breakthrough curves were compared with theoretical ones based on an axially dispersed plug flow through the column and the linear driving force rate equation. In addition, different semi-predictive multi-component equilibrium equations were used for the breakthrough modeling: Langmuir 1, Langmuir 2 and Langmuir-Freundlich extended models. The overall mass transfer coefficients were derived by matching theoretical with experimental breakthrough curves for single component systems, i.e., water vapor or SO_2 in a carrier gas. They were also predicted from a simplified bi-porous adsorbent model and compared with experimentally derived values. The presence of CO_2 species in ternary mixtures with water vapor and SO_2, even at relatively high concentrations of 9 vol%, had no significant effect on the breakthrough behavior of the other two species. For that reason the CO_2 species was ignored in the analysis of the resulting pseudo binary mixtures. The breakthrough model was solved by finite element orthogonal collocation method using the commercial software gPROMS. Both extended Langmuir 1 and Langmuir 2 based models gave reasonable predictions of the water and SO_2 breakthrough curves for pseudo binary mixtures involving a mordenite sample for all water concentration levels used in this study (up to 3.5 vol%). However, the same models were successfully used to predict SO_2 breakthrough curves for a MFI sample only at low water concentrations, i.e., 1.5 vol%. At the higher water levels both models failed to describe equilibrium behavior in the MFI sample due to the introduction of multi-layer adsorption in the interstices between small MFI-26 crystals.

Keywords: adsorption, modeling, breakthrough curves, SO_2, roll-up effect

Introduction

Adsorption of SO_2 has been studied as an alternative technique to abate this pollutant species from flue gas by taking advantage of the roll-up effect. The previous studies carried out in 1970's (Ma and Mancel, 1972; Roux et al., 1973; Ma and Roux, 1973; Ma et al., 1978) focused on diffusion measurements of SO_2 and other gases that typically make up a flue gas mixture using mainly mordenite type zeolites (MOR) because of their stability under acidic conditions. A decade later (1980's), pentasyl type zeolites (MFI) became subject of intensive investigations, mainly because of their hydrophobic properties (Chen, 1976; Nakamoto and Takahashi, 1982; Chriswell and Gjerde, 1982; Gollakota and Chriswell, 1988). Based on the more recent studies (Stenger et al., 1993a, 1993b; Tantet et al., 1995; Dunn et al., 1996; Rouf and Eić, 1998) adsorption using hydrophobic zeolites of MOR and MFI types proved to be a potential process for flue gas desulfurization using the roll-up effect. This effect is characterized by the breakthrough overshoot (displacement) of the more weakly adsorbed species (SO_2) in the competition with the more strongly

*To whom correspondence should be addressed.

adsorbed species (H_2O), which results in a multifold increase of the effluent SO_2 concentration in comparison with its original concentration in the feed. This could lead to the potential use of adsorption as the concentration step (initial step) before the final treatment in a more conventional unit, for example, a wet scrubber.

In general adsorption of ternary mixtures consisting of SO_2, H_2O and CO_2 species in nitrogen as a carrier gas on MFI and MOR type zeolites was found to be essentially unaffected by the presence of CO_2 (Mello, 2000). For that reason ternary mixtures in this study are designated as pseudo binary mixtures, and this term will be used throughout the article.

The main objective in this study was focused on proposing a simple mathematical model for the analysis of SO_2 and H_2O breakthrough curves from their respective pseudo binary mixtures. For that purpose non-iterative equilibrium models for predicting mixed gas adsorption were chosen, i.e., extended Langmuir 1 and 2 and extended Langmuir-Freundlich models. Equilibrium parameters for the extended model equations were derived from the appropriate single component experimental isotherms. In addition, a simple bi-porous model was used for the analysis of mass transfer and determination of overall mass transfer coefficients. Inherent to the model are assumptions of axially dispersed plug flow and isothermal operating conditions.

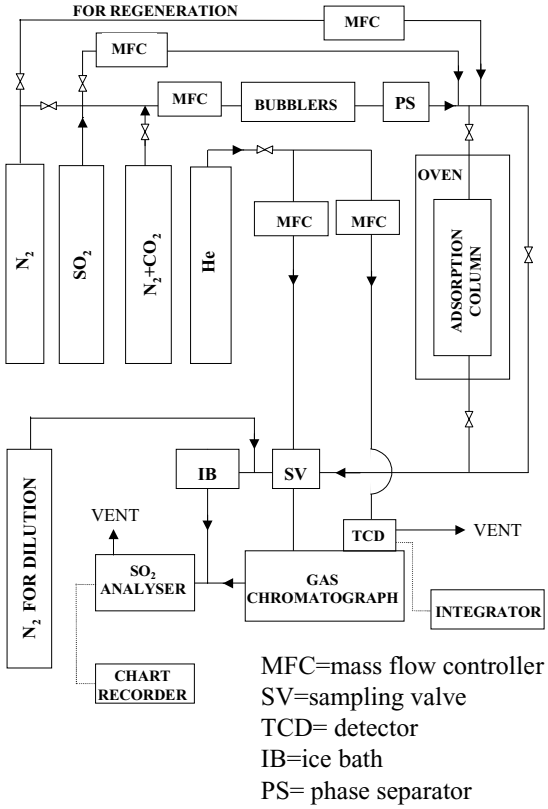

Figure 1. Experimental set-up for the breakthrough curve measurements.

Experimental

Experimental Set-up and Procedures

Breakthrough curves were obtained by feeding the gas mixture into the adsorption column packed with the fresh zeolite sample and measuring the effluent concentration of each sorbate species as a function of time. The mixtures used in this study contained water vapor in concentrations of 1.5, 2.5 and 3.5 vol%, sulfur dioxide concentrations of 950 and 1800 ppmv and CO_2 concentration of about 9 vol%. Table 1 provides a list of the pseudo binary mixtures. A typical flow-rate of 170 scm^3/min., temperature of 50°C and atmospheric pressure were used in the experiments. The regeneration of zeolite samples was carried out at relatively high temperature (300°C) under the pure nitrogen purge (typically 60 scm^3/min) over 8–12 hour period.

Table 1. Pseudo binary mixtures used in this study.

Mixture	SO_2 (ppmv)	H_2O (vol%)	CO_2 (vol%)
1	1800	1.5	∼9
2	1800	2.5	∼9
3	1800	3.5	∼9
4	950	3.5	∼9

The experimental apparatus, shown in Fig. 1, comprised two main gas lines: the main line which contained a mixture of 10 vol% CO_2 in nitrogen, and the other line introducing a mixture of 2.33 vol% SO_2 in nitrogen into the main line. The gas flow-rates were measured by mass flow controllers (models Matheson and Brooks). Water vapor was added by passing the gas mixture through two bubblers connected in series and placed in a thermostatic bath. The temperature of the bath was adjusted to provide the desired water vapor concentration in the gas mixture. A phase separator was installed after the bubblers to eliminate water droplets from the stream fed to the column. The adsorption column was placed in an oven which was maintained at 50°C. The 13 cm long and 0.78 cm diameter column

was made of stainless steel tube with polished inside wall.

Water vapor and CO_2 concentrations were measured by a thermal conductivity detector attached to a gas chromatograph (Varian 3400). A six-port sampling valve (Valco Instruments Co. Corp.) actuated by air and controlled by the gas chromatograph, was used to take samples of the gas mixture at programmed time intervals. The sample was then fed to an analytical column (Haysep D), provided by Chromatographical Specialties that has high selectivity for H_2O and CO_2 species. Helium was used as the carrier gas during the sampling procedure. The effluent SO_2 concentrations were measured separately by an infrared analyzer (Siemens, model ULTRAMAT 21 P).

Areas under the peaks for water and SO_2 were evaluated by an integrator attached to the gas chromatograph. Before starting the experiments as outlined above, the linearity of the detector was checked by obtaining chromatographic peaks and their respective areas using different concentrations of water and CO_2.

Experimental isotherm data for SO_2, H_2O and CO_2 were obtained from the CAHN (D-200) digital microbalance using a standard gravimetric procedure. The particle pore size distribution was determined in the Autosorb instrument (Quantachrome Inc.) using standard nitrogen adsorption at 77 K.

Most of the experimental runs were repeated in order to confirm desired reproducibility of the obtained results (generally very little scatter of the data between the runs was observed).

Sample Preparations

The samples used in this paper, MFI-26 ($SiO_2/Al_2O_3 = 26$) and MOR-20 ($SiO_2/Al_2O_3 = 20$) were kindly provided by PQ Corporation and were supplied in the form of very fine powder. In order to avoid a significant pressure drop across the column the powder was agglomerated in pellets applying pressure of 3000 psi. No binder was used in the agglomeration process. The pellets were then crushed and sieved, and the fraction between mesh 8 and 14 was collected for the experiments. The average pellet had a diameter of $d_p = 0.18$ cm.

Breakthrough Modeling

The breakthrough model used in this study is based on differential mass balance for the axially dispersed plug flow involving a trace system (Eq. (1)), with accompanying boundary and initial conditions (Arumugam et al., 1999; Ruthven, 1984). The boundary conditions for the mass balance were given by Danckwerts (Ruthven, 1984; Eqs. (2) and (3), respectively) along with the initial conditions for a clean bed prior to the experiment (Eqs. (4) and (5)).

$$\varepsilon_c \frac{\partial c_i}{\partial t} - \varepsilon_c D_L \frac{\partial^2 c_i}{\partial z^2} + \varepsilon_c v \frac{\partial c_i}{\partial z} + (1-\varepsilon_c)\frac{\partial q_i}{\partial t} = 0 \quad (1)$$

$z = 0$:

$$-\varepsilon_c D_L \frac{\partial c_i(0,t)}{\partial z} = v[c_{i,o} - c_i(0,t)] \quad (2)$$

$z = L$:

$$\frac{\partial c_i(L,t)}{\partial z} = 0 \quad (3)$$

$$c_i(0,z) = 0 \quad (4)$$

$$q_i(0,z) = 0 \quad (5)$$

The axial dispersion coefficient was calculated using the expression proposed by Edwards and Richardson (1968):

$$\frac{D_L}{2vR_p} = \gamma_1 \frac{D_m}{2vR_p} + \frac{1}{Pe_\infty \frac{1+\beta\gamma_1 D_m}{2vR_p}} \quad (6)$$

with $\gamma_1 = 0.73$, $\beta = 13.0$ and $Pe_\infty = 2.0$.

The mass transfer rate was expressed using the linear driving force model (Ruthven, 1984; Glueckauf and Coates, 1947):

$$\frac{\partial q_i}{\partial t} = k_i(q_i^* - q_i) \quad (7)$$

The overall mass transfer coefficients (k_i) for different species were determined by matching the single component breakthrough model with appropriate experimental data. They could also be predicted from a simplified bi-porous adsorbent model for the pellet (Ruthven, 1984):

$$\frac{1}{k_i K_i} = \frac{R_p}{3k_{f,i}} + \frac{R_p^2}{15\varepsilon_p D_{eff,i}} + \frac{r_c^2}{15K_i D_{c,i}} \quad (8)$$

where K_i in Eq. (8) is defined on a dimensionless particle volume basis, i.e., Henry Law constant in the linear region or simply q_o^*/c_o in the non-linear region of an isotherm.

The effective diffusivity (D_{eff}) is defined as:

$$D_{eff} = \frac{D_p}{\tau} \tag{9}$$

where τ is a tortuosity factor determined experimentally from the uptake data (Mello, 2000).

A similar approach was used by Tantet et al. (1995) and Rouf and Eić (1998) for the modeling of SO_2 and H_2O breakthrough curves in earlier studies.

The following extended equilibrium models were used in combination with the general model (Eqs. (1)–(7)):

1. Extended Langmuir 1 model

$$\frac{q_i^*}{q_{m,i}} = \frac{b_i c_i}{1 + \sum_{i=1}^{N} b_i c_i} \tag{10}$$

2. Extended Langmuir-Freundlich:

$$\frac{q_i^*}{q_{m,i}} = \frac{b_i c_i^{n_i}}{1 + \sum_{i=1}^{N} b_i c_i^{n_i}} \tag{11}$$

3. Extended Langmuir 2:

$$q_i^* = \frac{b_{i,1} q_{mi,1} c_i}{1 + \sum_{i=1}^{N} b_{i,1} c_i} + \frac{b_{i,2}\, q_{mi,2} c_i}{1 + \sum_{i=1}^{N} b_{i,2} c_i} \tag{12}$$

The equilibrium parameters for the Langmuir 1 model were extracted by a linear regression analysis using the standard p_i/q_i^* vs. p_i plots, while Langmuir 2 and Langmuir-Freundlich parameters were determined from a non-linear regression using the Sigma Plot 5.0 software (Mello, 2000).

Equations (1)–(7), together with one of the equilibrium isotherms (Eqs. (9)–(11)) were solved simultaneously for SO_2 and H_2O species using finite elements orthogonal collocation method (OCFEM) as well as centered finite difference method (CFDM). The software gPROMS was used for this task. The accuracy of the numerical solution was verified by changing the grid size, the time step and the numerical method. The order of polynomial approximation of each method was also a very important parameter. Because of its relatively higher complexity, Langmuir 2 based model usually required a polynomial solution of fourth order (Mello, 2000).

Prediction of Equilibrium Capacities in the Pseudo Binary Mixtures

It was experimentally confirmed that the presence of CO_2 in the ternary mixtures had a negligible effect on the equilibrium capacity and breakthrough behavior of SO_2 and H_2O species even at the relatively high concentrations of CO_2 used in this study (Mello, 2000), and its effects were ignored in this and subsequent analyses. Similar observations were found in earlier studies (Rouf and Eić, 1998; Tantet et al., 1995; Stenger et al., 1993b).

MOR-20 Sample

Table 2 shows comparisons between experimental adsorption capacities obtained from the breakthrough measurements and those predicted by the equilibrium models used for SO_2 and H_2O/MOR-20 systems. The parameters for the extended models were extracted from the single component experimental isotherms, i.e., Langmuir 1 and 2 as shown in Fig. 2 and presented in Tables 3 and 4. Experimental data for SO_2 and most of the data for H_2O were obtained from the CAHN microbalance measurements. However, two additional data points for the water isotherm obtained from the single component breakthrough measurements were

Table 2. Comparison between experimental and predicted equilibrium adsorption capacities for water and SO_2 from respective pseudo binary mixtures on MOR-20 at 50°C.

Mixture (SO_2 in ppmv, H_2O in vol%)	Breakthrough experiment (mg/g)		Extended Langmuir 1 (mg/g)		Extended Langmuir 2 (mg/g)		Extended Langmuir-Freundlich (mg/g)	
	SO_2	H_2O	SO_2	H_2O	SO_2	H_2O	SO_2	H_2O
1800 ppmv, 1.5 vol%	4.5	77.5	5.8	74.2	3.1	89.6	18.1	80.4
1800 ppmv, 2.5 vol%	3.9	90.8	3.8	88.8	2.2	100.5	15.8	91.3
1800 ppmv, 3.5 vol%	3.1	99.4	2.8	97.0	1.6	106.3	14.4	98.4
950 ppmv, 3.5 vol%	1.8	98.5	1.5	100.1	0.9	106.8	10.0	101.0

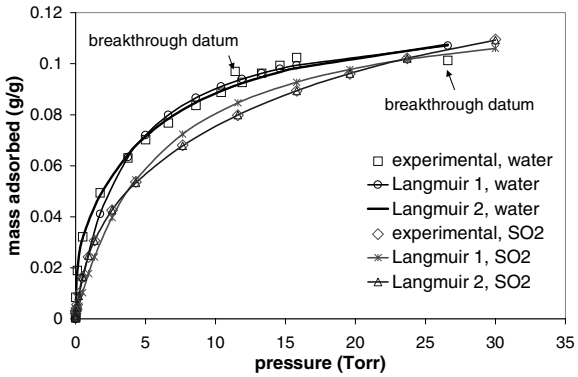

Figure 2. Experimental isotherms and Langmuir 1 and 2 fittings for the systems water/MOR-20 and SO_2/MOR-20 at 50°C.

added to the gravimetric data to show: comparison with the microbalance (gravimetric) data (medium pressure point) and to extend the isotherms beyond the microbalance measurement range in order to include the pressure datum corresponding to 3.5 vol% (Mello, 2000). The isotherms for both species showed type I behavior (Fig. 2) according to Brunauer classification (Sing, 1997; Sing et al., 1985). In order to eliminate uncertainties related to energy heterogeneity of adsorption sites at very low pressures, experimental data in that region for both H_2O and SO_2 isotherms were discarded. However, all data of relevance were analyzed including a relatively low pressure range of 0.7–1.5 Torr that corresponds to a typical mixture content of SO_2 species investigated in this study. Although both Langmuir 1 and 2 single models generally provided good fit of the experimental isotherm data, the two-site Langmuir 2 model proved to be somewhat more successful in describing the equilibrium behavior (Fig. 2). The Langmuir-Freundlich isotherm, on the other hand, was successful to describe the water isotherm, but proved inadequate for the SO_2 isotherm (Mello, 2000). Contrary to expectations, based on the single component analyses, extended Langmuir 1 model gave better predictions for both SO_2 and water adsorption capacities as shown in the Table 2. However, very good predictions obtained by the Langmuir 1 extended model do not necessarily reflect the best applicability of that model to adequately describe $SO_2$and water behaviors for the entire concentration (pressure) range, since the single-component Langmuir 1 isotherm was less satisfactory in describing the single component equilibrium isotherms than the Langmuir 2. Therefore good predictions by the extended Langmuir 1 isotherm shown in Table 2 are probably fortuitous. Finally, the Langmuir-Freundlich extended model provided good predictions for water and very poor predictions for SO_2 as was expected based on the single component analysis.

Table 3. Langmuir 1 model parameters for water and SO_2 adsorption on MOR-20 at 50°C.

Sample	Sorbate	b [g/(g.Torr)]	q_m (g/g)
MOR-20	water	0.2954	0.1207
	SO_2	0.1765	0.1260

Table 4. Langmuir 2 model parameters for water and SO_2 adsorption on MOR-20 at 50°C.

Sample	Sorbate	b_1 [g/(g.Torr)]	q_{m1} (g/g)	b_2 [g/(g.Torr)]	q_{m2} (g/g)
MOR-20	Water	100.0	0.0041	0.8	0.095
	SO_2	57.7	0.0051	0.6	0.069

MFI-26 Sample

One additional experimental single component breakthrough datum is included in the water isotherm to extend it beyond the microbalance measurement range, and to include the partial pressure corresponding to 3.5 vol% concentration (Fig. 3). While the SO_2 adsorption follows the typical Type I isotherm, the shape of the water isotherm clearly indicates monolayer- multilayer adsorption followed by capillary condensation typical of the Type IV behavior.

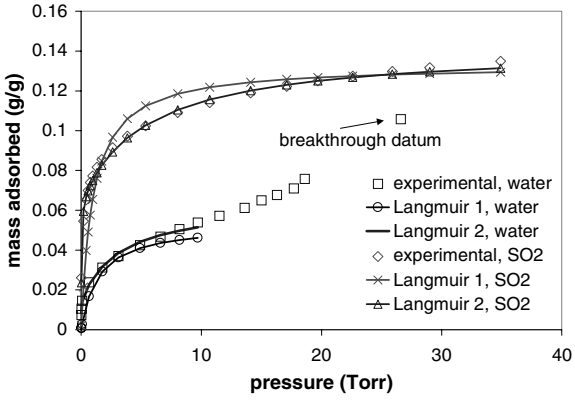

Figure 3. Experimental isotherms and Langmuir 1 and 2 fittings for the systems water/MFI-26 and SO_2/MFI-26 at 50°C.

Table 5. Experimental equilibrium adsorption capacities and selected predictions for water and SO_2 from respective pseudo binary mixtures on MFI-26 at 50°C (predicted data only for the mixture: 1800 ppmv SO_2 and 1.5 vol% water).

Mixture (SO_2 in ppmv, H_2O in vol%)	Breakthrough experiment (mg/g)		Extended Langmuir 1 (mg/g)		Extended Langmuir 2 (mg/g)		Extended Langmuir-Freundlich (mg/g)	
	SO_2	H_2O	SO_2	H_2O	SO_2	H_2O	SO_2	H_2O
1800 ppmv, 1.5 vol%	5.4	53.7	17.2	44.4	7.8	50.1	32.9	56.5
1800 ppmv, 2.5 vol%	4.8	84.8	–	–	–	–	–	–
1800 ppmv, 3.5 vol%	3.8	100.1	–	–	–	–	–	–
950 ppmv, 3.5 vol%	2.3	100.8	–	–	–	–	–	–

The pore size distribution of the particles, carried out in the Autosorb instrument showed the presence of both micropores ($0 < d_p < 20$ Å, according to Dubinin-Radushkevich analysis) and, to a lesser extent, mesopores ($20 < d_p < 500$ Å). The mesopore size distribution, determined by the Barrett, Joyner and Halenda (BJH) model indicates the existence of mesopores, with the most significant peaks occurring at pore diameter ranging from 20 to 50 Å (Mello, 2000). The mesopore and micropore cumulative volumes were found to be 0.015 and 0.35 cm^3/g of adsorbent respectively, which indicates that the mesopore volume corresponds to about 4% of the total micropore-mesopore volume. Since identical water isotherms were obtained for both powdered and pelleted MFI-26 samples (Mello, 2000), it was concluded that the mesopores were formed in the intermediate zeolite structure due to the existence of interstices between small MFI-26 crystals. The multi-layer adsorption starts in these interstices at the pressure of about 12 Torr followed by the capillary condensation at the higher pressure of about 20 Torr (Fig. 3). The latter pressure corresponds to a relative pressure of about 0.22 for the water vapor at 50°C, which is very close to the relative pressure of 0.25 considered to be a critical value at which capillary condensation starts to occur in the interstices (Ruthven, 1995). At still higher relative pressures, significant multi-layer adsorption on the external surfaces of the small crystals can also occur. Due to the complexity of this problem which has resulted from the superficial water adsorption on the intermediate porous structure as describe above, the extended Langmuir 1 and 2 models were only used for the analysis of the initial portion of the water isotherms (up to the pressures of 10–12 Torr). As a result of that constraint, only the analysis involving pseudo binary mixtures with low water concentration, i.e., 1.5 vol% (corresponds to a partial pressure of about 11 Torr) was performed.

The same approach of discarding unreliable low pressure points from the respective isotherms was carried out for the MFI-26 sample. In this case, Langmuir 2 model provided a more successful fit of the experimental isotherm data than the Langmuir 1 model for both sorbates, as depicted in Fig. 3. The Langmuir-Freundlich isotherm, on the other hand, was successful to describe the SO_2 isotherm, but proved inadequate for the water isotherm (Mello, 2000). Table 5 shows comparisons between the experimental breakthrough equilibrium capacities for all pseudo binary mixtures and those predicted by the extended models for the mixture containing 1.5 vol% of water. Based on the single component analyses, Langmuir 2 extended model gave better predictions for both SO_2 and water adsorption capacities whereas Langmuir 1 and, in particular, Langmuir-Freundlich extended models significantly overpredicted the adsorption capacities for SO_2 in the pseudo binary mixtures. Therefore the extended Langmuir 2 isotherm was considered to be the most adequate for the breakthrough modeling of MFI-26 sample.

Overall Mass Transfer Coefficients

The overall mass transfer coefficients (k_i) for SO_2 and H_2O species were determined by matching the theoretical breakthrough curves with the experimental data for single component systems (Mello, 2000). Thus obtained values were used in modeling of the pseudo binary mixtures. In addition, these values were combined with equilibrium constants K to calculate the experimental overall mass transfer resistances ($1/kK$) as shown in Tables 6 and 7 (last columns), and then compared to the theoretical predictions calculated from the bi-porous model (Eq. (8)). The results presented in Tables 6 and 7 show that the overall mass transfer

Table 6. Comparisons between experimental and predicted overall mass transfer resistances for water on MOR-20 and MFI-26 zeolites at 50°C.

Sorbate Water	Experimental tortuosity factor, τ Unitless	Macropore resistance (1) $R_p^2/15\varepsilon_p D_{eff}$ (sec)	Fluid film resistance (2) $R_p^2/3k_f$ (sec)	Predicted overall resistance (1) + (2) $1/kK$ (sec)	Experimental overall mass transfer coefficient k (sec^{-1})	Experimental overall resistance $1/kK$ (sec)
			MOR-20			
1.5 vol%	4.5	0.037	0.004	0.041	0.003	0.037
2.5 vol%	4.5	0.037	0.004	0.041	0.003	0.049
3.5 vol%	4.5	0.037	0.004	0.041	0.004	0.052
			MFI-26			
1.5 vol%	3.0[a]	0.027	0.004	0.031	0.007	0.038

[a]Assumed value.

Table 7. Comparisons between experimental and predicted overall mass transfer resistances for SO_2 on MOR-20 and MFI-26 zeolites at 50°C.

Sorbate SO_2	Experimental tortuosity factor, τ Unitless	Macropore resistance (1) $R_p^2/15\varepsilon_p D_{eff}$ (sec)	Fluid film resistance (2) $R_p^2/3k_f$ (sec)	Predicted overall resistance (1) + (2) $1/kK$ (sec)	Experimental overall mass transfer coefficient k (sec^{-1})	Experimental overall resistance $1/kK$ (sec)
			MOR-20			
1800 ppmv	3.5	0.053	0.006	0.059	0.003	0.059
			MFI-26			
1800 ppmv	2.2	0.037	0.006	0.045[a]	0.004	0.045

[a]Includes the micropore mass transfer resistance (0.002 sec) that was measured for this system.

process is macropore controlled for both sorbates. Effective diffusivities for macropore resistances (third column) were calculated from Eq. (9) using tortuosity values (second column in the tables) determined from the uptake experimental data (Mello, 2000), except for the water/MFI-26 system where an average value of 3 was taken (Rouf and Eić, 1998). The pore diffusivity in the Eq. (9) was calculated using a simple additivity law for mass transfer resistances due to molecular and Knudsen diffusion in secondary pore (mesopore) structure. The micropore resistances for some systems, i.e., water and SO_2 in MFI-26 single crystals were determined experimentally and found negligible (Mello, 2000), which was expected due to the small size of the single crystals used to form the pellets (1–2 μm). These resistances were also assumed to be negligible for MOR-20 and therefore ignored in all calculations (only first two terms of Eq. (8) were used).

The bi-porous model very successfully predicted overall mass transfer resistances for the SO_2 adsorption on zeolites used in this study (Table 7). Reasonable agreements were also obtained for the water adsorption (Table 6). Some discrepancy between the theoretical and experimental values are noticeable for higher water concentrations, i.e., 2.5 and 3.5 vol% in MOR-20. This could be attributed to surface diffusion in the larger pores due to capillary condensation of water in the mesopores. This is likely to become a more pronounced effect as the water concentration is increased, as shown in Table 6 by the increased trend of experimentally determined overall resistances. The results for 1.5 vol% water in MFI-26 sample are also in a reasonable agreement.

Based on the above analysis it is reasonable to expect that the bi-porous model could be successfully used for the prediction of mass transfer coefficients in future modeling involving similar gas mixtures.

Breakthrough Curves

Both Langmuir 1 and 2 equilibrium relations were successfully used for the breakthrough modeling of water and SO_2 involving MOR-20 sample. However, Langmuir 1 based model gave somewhat better agreements with experimental curves for MOR-20 due to more successful equilibrium predictions of the pseudo binary mixtures as discussed in the preceding sections.

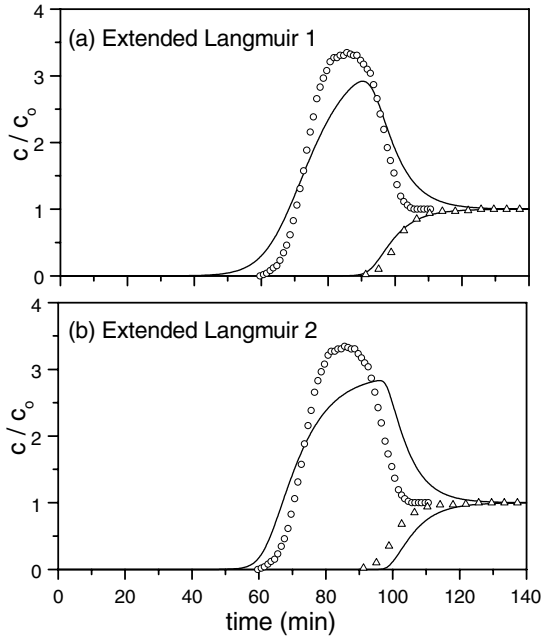

Figure 4. Experimental and predicted breakthrough curves for SO_2 and H_2O on MOR-20 at 50°C for the pseudo binary mixture of 1800 ppmv SO_2 and 2.5 vol% H_2O (a) Extended Langmuir 1 based model and (b) Extended Langmuir 2 based model.

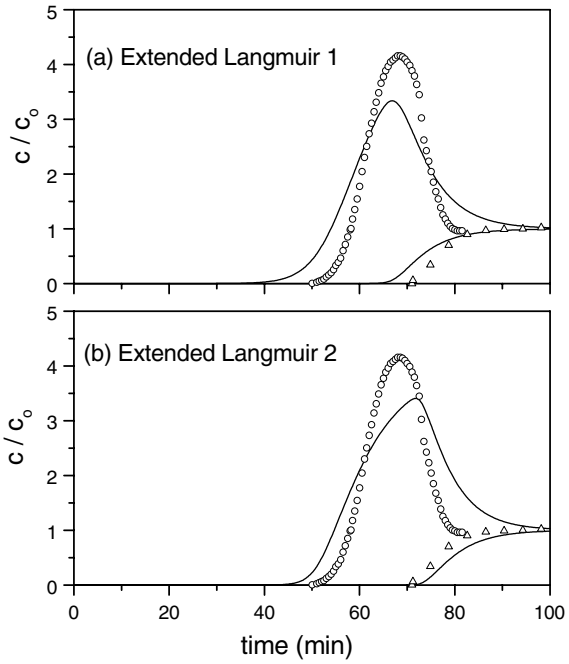

Figure 5. Experimental and predicted breakthrough curves for SO_2 and H_2O on MOR-20 at 50°C for the pseudo binary mixture of 1800 ppmv SO_2, and 3.5 vol% H_2O (a) Extended Langmuir 1 based model and (b) Extended Langmuir 2 based model.

On the other hand the Langmuir 2 was found to be the most suitable for the equilibrium predictions involving MFI-26, and was therefore used for modeling of this zeolite. Figures 4 and 5 give a summary of theoretical breakthrough curves in comparison with the experimental data for MOR-20 sample. Figure 6 shows comparisons of predicted and experimental breakthrough curves for MFI-26 sample at relatively low concentration of water, i.e., 1.5 vol%. As discussed in the equilibrium section, the Langmuir models were found inappropriate to describe multi-layer adsorption that occurred at the higher water concentration levels in the MFI type sample.

In striking contrast to SO_2, the water breakthrough curves resemble those of the single component systems indicating negligible effects of SO_2 on the other species' breakthrough behavior. On the other hand competitive adsorption in the binary mixture led to the unusually high water-driven roll up effect in the SO_2 breakthrough curves. In all cases involving the roll-up effects the models correctly predicted the general trend and shape of these curves which is somewhat surprising given the relative simplicity of the models used to describe complex processes involving

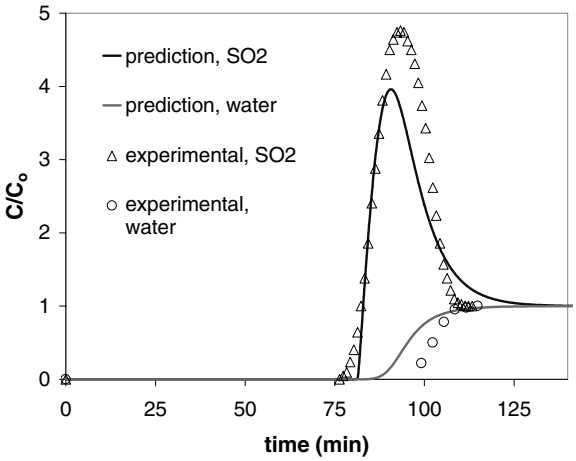

Figure 6. Experimental and predicted breakthrough curves for SO_2 and H_2O on MFI-26 at 50°C for the pseudo binary mixture of 1800 ppmv SO_2, and 1.5 vol% H_2O using the Extended Langmuir 2 based model for predictions.

strong effects of water adsorption and displacement of SO_2 species. However, the models under-predicted the height of roll-up effects. This could be attributed to strong heat effects especially at higher water concentrations, i.e., 3.5 vol%, thus producing more

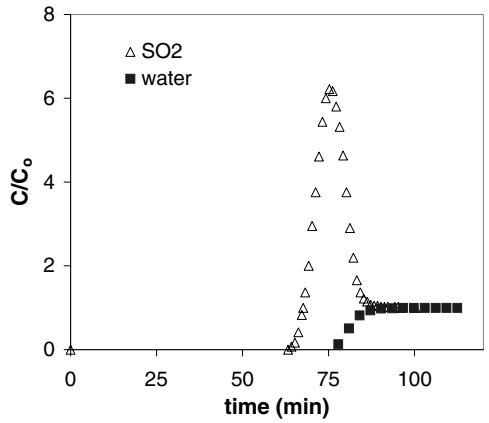

Figure 7. SO_2 and H_2O experimental breakthrough curves for the pseudo binary mixture containing 1800 ppmv SO_2 and 3.5 vol% H_2O on MFI-26 at 50°C.

pronounced non-equilibrium conditions, and causing more efficient SO_2 displacement. To try to resolve these discrepancies a non-isothermal model should be considered for the more appropriate modeling in future.

To assess the role of water concentration on the roll-up effect of SO_2, Fig. 7 shows experimental breakthrough curves for SO_2 and H_2O in MFI-26 sample for the pseudo binary mixture containing 3.5 vol% of water and 1800 ppmv of SO_2(no theoretical curves are presented because of inadequacy of extended isotherms as discussed above). It is obvious that the roll-up effect becomes more pronounced as the water concentration in the mixtures is increased, which is expected due to the fact that water is a more strongly adsorbed species.

The FTIR analysis reported in our earlier study (Mello et al., 2001) provides further evidence of the significant displacement of SO_2 by H_2O in the adsorption sites. This analysis has revealed that water is always more strongly hydrogen bonded to the surface hydroxyls than SO_2. Thus, strongly polar water molecules cause the SO_2, which has weaker hydrogen bonds, to be effectively displaced (roll-up effect) especially at the higher partial pressures of water vapor (Mello, 2000; Rouf and Eić, 1998; Tantet et al., 1995; Stenger et al., 1993b).

Conclusions and Recommendations

The multi-component isothermal breakthrough model represented by an axially dispersed plug flow, the linear driving force equation and the extended Langmuir 1 and 2 isotherms (MOR) and extended Langmuir 2 isotherm (MFI) generally proved successful in predicting the experimental breakthrough curves. The prediction of the breakthrough curves reflected the adequacy of the equilibrium models to represent the adsorption capacities in the pseudo binary mixture. For MOR-20 systems both extended Langmuir 1 and 2 models generally gave good predictions of SO_2 and water equilibrium capacities in the pseudo binary mixtures, although Langmuir 1 model was somewhat more successful. Contrary to this, only Langmuir 2 model was successful to characterize the MFI-26 systems reasonably well until the onset of multi-layer adsorption (up to pressure of 10 Torr). The roll-up effects were generally underpredicted, which is most likely due to the existence of non-equilibrium conditions caused by relatively high heat effects from water adsorption, thus enhancing SO_2 displacement. It is recommended that a non-isothermal model be used in the future studies to address this effect more properly.

Mass transfer coefficients were extracted by matching an appropriate breakthrough model with experimental curves involving single component systems. These values were compared with predicted results using a simple bi-porous model for agglomerated particles. Due to relatively good agreements between experimental and predicted values a future use of the bi-porous model is recommended in breakthrough modeling of the similar systems.

The study showed existence of a great potential for the concentration of SO_2 from typical combustion flue gases using roll-up effect, which could significantly affect techno-economical performance of a scrubber unit being used for the removal of this species.

Nomenclature

b_i	Langmuir or Langmuir-Freundlich extended model parameter for component i (m^3/mol)
$b_{i,1}$ and $b_{i,2}$	Extended Langmuir 2 model parameters for component i in sites 1 and 2, respectively (m^3/mol)
c_i	Molar concentration of sorbate i in gas phase (mol/m^3)
$c_{i,o}$	Initial molar concentration of sorbate i in gas phase (mol/m^3)
d_p	Average pellet diameter (m)
$D_{c,i}$	Micropore diffusion coefficient for component i (m^2/sec)

$D_{eff,i}$	Effective diffusion coefficient for component i (m^2/sec)
D_L	Axial dispersion coefficient (m^2/sec)
$D_{m,i}$	Molecular diffusion coefficient for component i (m^2/sec)
$D_{p,i}$	Macropore diffusivity for component i (m^2/sec)
k_i	Overall mass transfer coefficient for component i (sec^{-1})
$k_{f,i}$	External film mass transfer coefficient for component i (m^2/sec)
K_i	Volume based adsorption constant for component i, dimensionless
L	Column length (m)
n_i	Extended Langmuir-Freundlich model parameter for component i, dimensionless
Pe_∞	Limiting value of Peclet number, dimensionless
q_i	Adsorbed phase concentration of component i (mol/m^3)
$q_{m,i}$	Monolayer capacity for component i (kg sorbate/kg adsorbent)
$q_{mi,1}$ and $q_{mi,2}$	Monolayer capacity for component i in sites 1 and 2, respectively in Langmuir 2 model (kg sorbate/kg adsorbent)
q_i^*	Equilibrium concentration for component i in the adsorbed phase (mol/m^3 or kg sorbate/kg adsorbent)
r_c	Crystal radius (m)
R_p	Pellet radius (m)
z	Axial coordinate (m)

Greek Letters

ε_c	Column porosity
ν	Interstitial velocity (m/sec)
γ_1	Parameter in Eq. (6), dimensionless
β	Parameter in Eq. (6), dimensionless
τ	Tortuosity factor, dimensionless

Acknowledgments

The authors gratefully acknowledge CAPES (Coordenadoria para Aperfeiçoamento de Pessoal de Nível Superior of the Government of Brazil), and NSERC (Natural Sciences and Engineering Research Council of Canada) for the financial support provided for this project. Special thanks are due to Dr. Ming Jiang for his help provided for the simulation of some experimental data.

References

Arumugam, B.K., J.F. Banks, and P.C. Wankat, "Pressure Effects in Adsorption Systems," *Adsorption*, **5**, 261–278 (1999).

Chen, N.Y., "Hydrophobic Properties of Zeolites," *J. Phys. Chem.*, **80**(1), 60–63 (1976).

Chriswell, C.D. and D.T. Gjerde, "Sampling of Stack Gas for Sulfur Dioxide with a Molecular Sieve Adsorbent," *Anal. Chem.*, **54**, 1911–1913 (1982).

Do, D.D., *Adsorption Analysis: Equilibria and Kinetics*, ch. 6, Imperial College Press, London, 1998.

Dunn, J.P., Y. Cai, S. Liebmann, H.G. Stenger, Jr., and D.R. Simpson, "A Test and Demonstration Unit for Concentrating Sulfur Dioxide from Flue Gas," *Ind. Eng. Chem. Res.*, **35**, 1409–1416 (1996).

Edwards, M.F. and J.F. Richardson, "Gas Dispersion in Packed Beds," *Chem. Eng. Sci.*, **23**, 109–123 (1968).

Glueckauf, E. and J.E. Coates, "Theory of Chromatography. Part IV. The Influence of Incomplete Equilibrium on the Front Boundary of Chromatograms and on the Effectiveness of Separation," *J. Chem. Soc*., 1315–1321 (1947).

Gollakota, S.V. and C.D. Chriswell, "Study of an Adsorption Process Using Silicalite for Sulfur Dioxide Removal from Combustion Gases," *Ind. Eng. Chem. Res*., **27**(1), 139–143 (1988).

Gregg, S.J. and K.S.W. Sing, *Adsorption, Surface Area and Porosity*, ch. 3, Academic Press, London, 1967.

Ma, Y.H. and C. Mancel, "Diffusion Studies of CO_2, NO, NO_2 and SO_2 on Molecular Sieves Zeolites by Gas Chromatography," *AIChE J.*, **18**(6), 1148–1153 (1972).

Ma, Y.H. and A.J. Roux, "Multicomponent Rates of Sorption of SO_2 and CO_2 in Sodium Mordenite," *AIChE J.*, **19**(5), 1055–1059 (1973).

Ma, Y.H., R.J. Byron, P. Feltri, and T.Y. Lee, "Effects of Presorbed Water Vapor upon the Sorption and Diffusion of Sulfur Dioxide in Natural Mordenites," *AIChE Symp. Ser.*, **74**(179), 48–52 (1978).

Mello, M., "Adsorption of Sulphur Dioxide from Multicomponent Mixtures on Hydrophobic Zeolites," Ph.D. Thesis, University of New Brunswick, Canada, 2000.

Mello, M., M. Eić, S. Hočevar, and U. Lavrenčič-Štangar, "Modeling of Sulfur Dioxide Breakthrough Curves from Ternary Wet Mixtures on MOR Type Zeolite," *Stu. Surf. Sci. Cat*. **135**; Also in *Zeolites and Mesoporous Materials at the Dawn of the 21st Century*, A. Galarneau, F. DiRenzo, F. Fajula, and J. Vedrine (Eds.), CD-ROM, Elsevier, Amsterdam, 2001.

Nakamoto, H. and H. Takahashi, "Hydrophobic Natures of Zeolite ZSM-5," *Zeolites*, **2**, 67–69 (1982).

Rouf, S. and M. Eić, "Adsorption of SO_2 from Wet Mixtures on Hydrophobic Zeolites," *Adsorption*, **4**, 25–33 (1998).

Roux, A., A.A. Huang, Y.H. Ma, and I. Zwiebel, "Sulfur Dioxide Adsorption on Mordenites," *AIChE Symp. Ser.*, **69**(134), 46–53 (1973).

Ruthven, D.M., *Principles of Adsorption and Adsorption Processes*, ch. 8, John Wiley & Sons, New York, 1984.

Ruthven, D.M., *Microporous Materials*, **22**, 537–541 (1998).

Sing, K.S.W., "Analysis of Physisorption Isotherms," in *Physical Adsorption: Experiment, Theory and Applications*, J. Fraissard

(Ed.), pp. 9–16, Kluwer Academic Publishers, Netherlands, 1997.

Sing, K.S.W., D.H. Everett, R.A.W. Haul, L. Moscou, R.A. Pierotti, J. Rouquerol, and T. Siemieniewska, "Reporting Physisorption Data for Gas/Solid Systems—with Special Reference to the Determination of Surface Area and Porosity," *Pure Appl. Chem*., **57**(4), 603–619 (1985).

Stenger Jr., H.G., K. Hu, and D. Simpson, "Competitive Adsorption of NO, SO_2 and H_2O onto Mordenite Synthesized from Perlite," *Gas Sep. and Purif.*, **7**(1), 19–25 (1993a).

Stenger Jr., H.G., K. Hu, and D. Simpson, "Chromatographic Separation and Concentration of Sulfur Dioxide in Flue Gases," *Ind. Eng. Chem. Res*., **32**(11), 2736–2739 (1993b).

Tantet, J., M. Eić, and R. Desai, "Breakthrough Study of the Adsorption and Separation of Sulfur Dioxide from Wet Gas Using Hydrophobic Zeolites," *Gas Sep. and Purif.*, **9**(3), 213–220 (1995).